Supplementary Information

Supplementary Figures 1-5. See separate file.

Supplementary Dataset 1. Mean per-gene extracted features for all channels of genome-wide screen

Supplementary Dataset 2. Features from single cells in secondary antibody screen. Available at Zenodo (https://doi.org/10.5281/zenodo.5013414).

Supplementary Dataset 3. Features from single cells in secondary reporter screen. Available at Zenodo (https://doi.org/10.5281/zenodo.5013414).

Supplementary Dataset 4. IRF3 translocation scores from primary and secondary IRF3 antibody and IRF3 reporter screens (the latter upon both Sendai virus and VSV infection) and SeV intensity scores from secondary antibody screen.

Supplementary Dataset 5. Peroxisome and Sendai virus feature scores from genome-wide screen

Supplementary Information

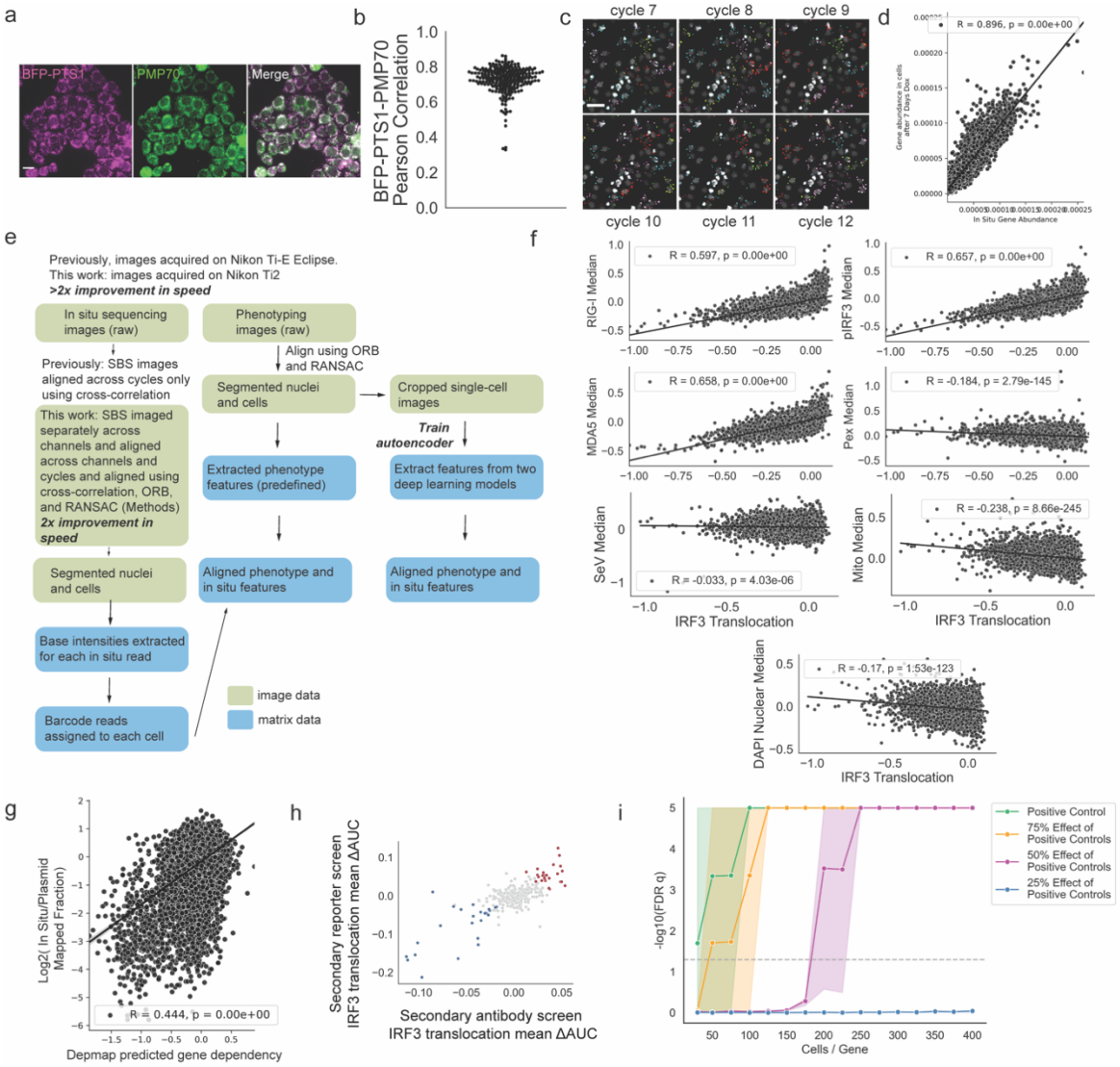

Supplementary Figure 1. (A) BFP-PTS1 in HeLa cells significantly overlaps with PMP70 antibody staining. Scale bar 20 μm. (B) Quantification of BFP-PTS1-PMP70 correlation in HeLa cells. (C) Remaining *in situ* sequencing cycles from Fig. 1d. (D) *In situ* gene abundance (combined sgRNA abundance) is highly correlated with gene abundance in cells after 7 days of doxycycline treatment. Pearson r correlation and two-tailed p value are denoted on plot (n = 20,389 genes). (E) Genome-wide screen image acquisition and analysis workflow, allowing for a >4-fold improvement in throughput over our previous optical pooled screening design. See Methods for further details. (F) RIG-I, pIRF3, and MDA5 intensities are significantly correlated with pIRF3 translocation levels, while peroxisome, mitochondria, and Sendai intensities are not positively correlated, indicating coordinated pathway responses. Pearson r correlations and two-tailed p values are denoted on plots (n = 19,093 genes). (G) Predicted Depmap dependency (1, 2) is significantly correlated with the *in situ* mapped gene-level fraction relative to the plasmid library mapped fraction. Pearson r correlation and two-tailed p value are denoted on plot (n = 15,917 genes). (H) Correlation between secondary screen translocation scores is significant (Pearson r = 0.74, two-tailed p = 4.7e-60, n = 342 genes). (I) Sensitivity analysis showing number of cells per gene required to significantly identify genes with effect sizes compared to those for strong positive controls *DDX58, MAVS,* and *IRF3.*

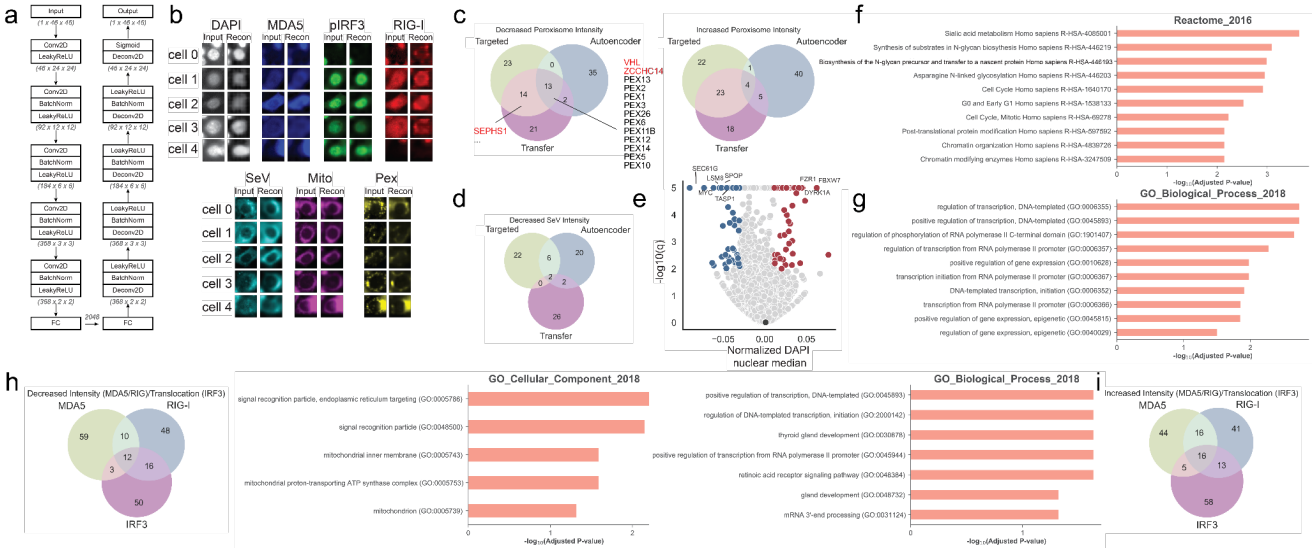

Supplementary Figure 2. (A) Architecture for an autoencoder used to extract 2048 features from images. (B) Example inputs and reconstructions for 5 single cells across 7 channels of interest. (C) Venn diagram showing overlap of top 50 genes using a targeted feature (decreased peroxisome intensity), autoencoder, or transfer learning. Overlapping genes are enriched for peroxisome biogenesis genes as well as *VHL,* and *ZCCHC14,* which were in the top 50 using all three feature sets, while *SEPHS1* was in the top 50 for all but the autoencoder features. (D) Venn diagram as shown in (C) but for genes that increased peroxisome intensity. (E) Volcano plot for genes affecting the DAPI nuclear median. Two-sided p-values were calculated as described in the Methods and corrected using the Benjamini-Hochberg procedure (n = 19,900 genes). (F) Significant Reactome terms for genes among the top 50 for decreased DAPI intensity in targeted, autoencoder, and transfer feature sets. Enrichr p-values are computed using the Fisher exact test and adjusted using the Benjamini-Hochberg procedure. (G) Significant GO BP terms for genes among the top 50 for increased DAPI intensity in targeted, autoencoder, and transfer feature sets. Enrichr p-values are computed using the Fisher exact test and adjusted using the Benjamini-Hochberg procedure. (H) Venn diagram of top genes from all feature sets showing decreased intensity (for MDA5/RIG-I) or translocation (IRF3) shows distinct genes influencing the receptors and IRF3. Genes uniquely affecting IRF3 are enriched for GO CC terms relating to mitochondria and ER, organelles likely affecting signaling downstream of PRRs, while genes uniquely decreasing RIG-I intensity are enriched for GO BP terms that include retinoic acid signaling, which the receptor is responsive to. Enrichr p-values are computed using the Fisher exact test and adjusted using the Benjamini-Hochberg procedure. (I) Venn diagram as in (H) showing genes that increased intensity or translocation for MDA5/RIG-I or IRF3, respectively.

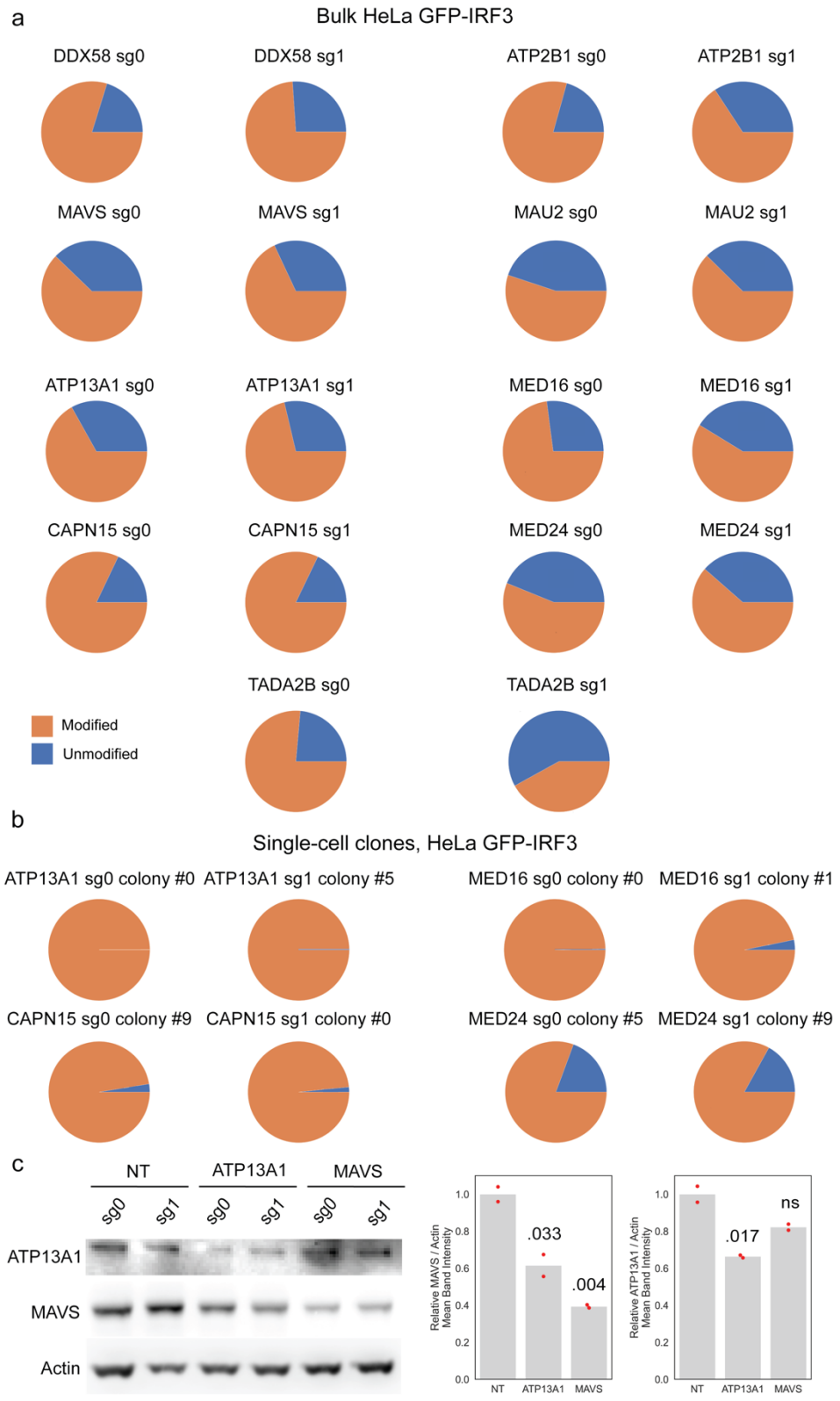

Supplementary Figure 3. (A) Crispresso analysis of amplicon sequencing for bulk knockouts of 10 genes in HeLa GFP-IRF3 cells shows a high proportion of edited sequences. (B) Crispresso analysis of edited sequence fraction for single-cell clones used in bulk RNA sequencing experiment. (C) Western blot shows a decrease in ATP13A1 and MAVS protein levels in the respective knockouts, p values calculated using Student's t-test.

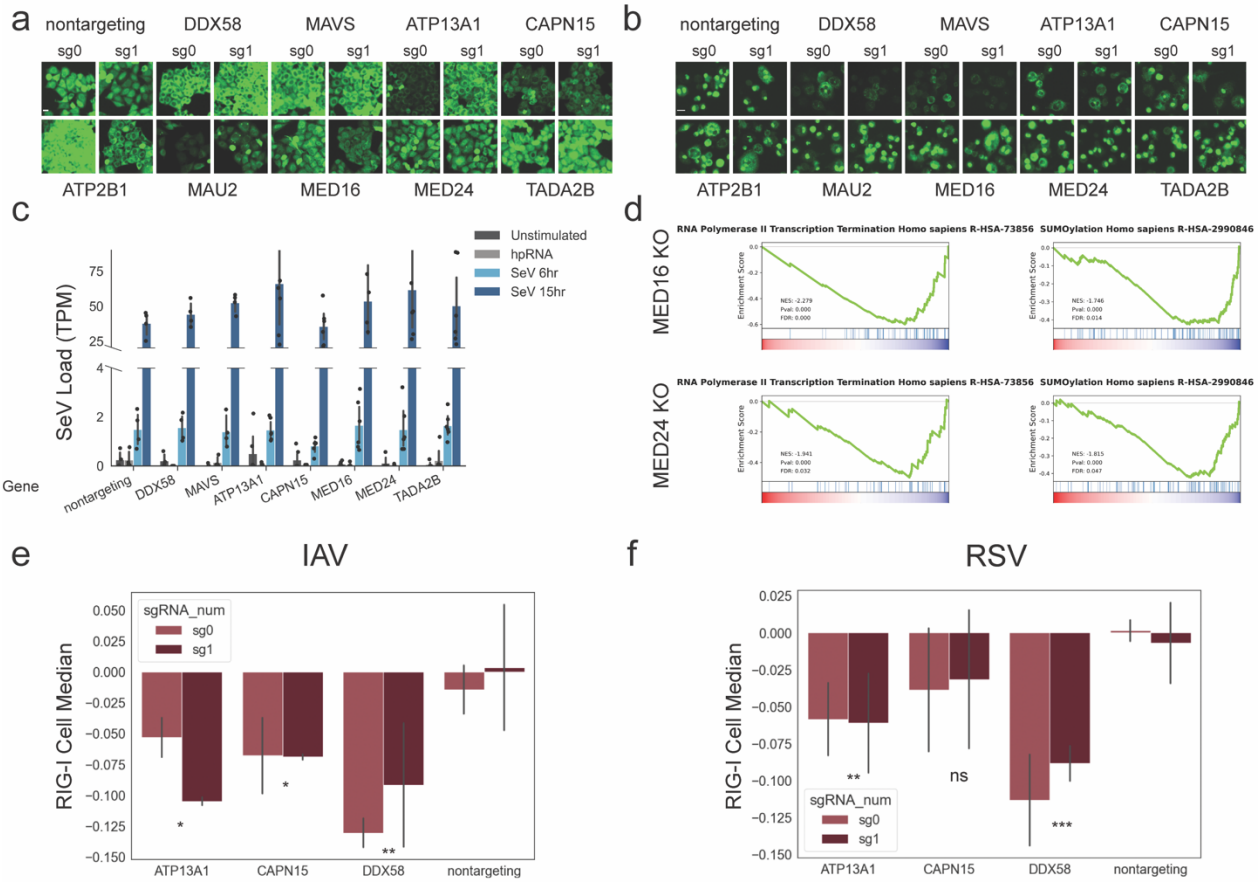

Supplementary Figure 4. (A) Representative images of cells from Fig. 4A. Scale bar 20 μm. (B) Representative images of cells from Fig. 4C. Scale bar 20 μm. (C) Sendai virus load measured by RNA-seq is not significantly different in genetic knockouts relative to non-targeting controls at either 6 hours or 15 hours post-infection. Significance was determined by assessing Benjamini-Hochberg adjusted p values from t tests between non-targeting and each sgRNA for each condition. (D). *MED16* and *MED24* GSEA results show significant decrease in RNA polymerase II transcription termination and SUMOylation. P-values were obtained from the gseapy package using 1000 permutations over all gene sets considered and corrected using the Benjamini-Hochberg procedure. (E) RIG-I intensities upon IAV infection in perturbed cells relative to non-targeting controls. Two-sided p-values for e/f were calculated by computing the delta AUC for RIG-I per-cell median intensity between cells in each well and non-targeting control cells (minimum n = 3,000); delta AUCs for all wells containing cells with an sgRNA of interest were then compared to non-targeting delta AUCs using a 2-sided t test, p values were combined using Fisher's method and corrected using the Benjamini-Hochberg procedure; * indicates $p < .05$, ** indicates $p < .01$. (F). RIG-I intensities upon RSV infection in perturbed cells relative to non-targeting controls; ** indicates $p < .01$, *** indicates $p < .001$.

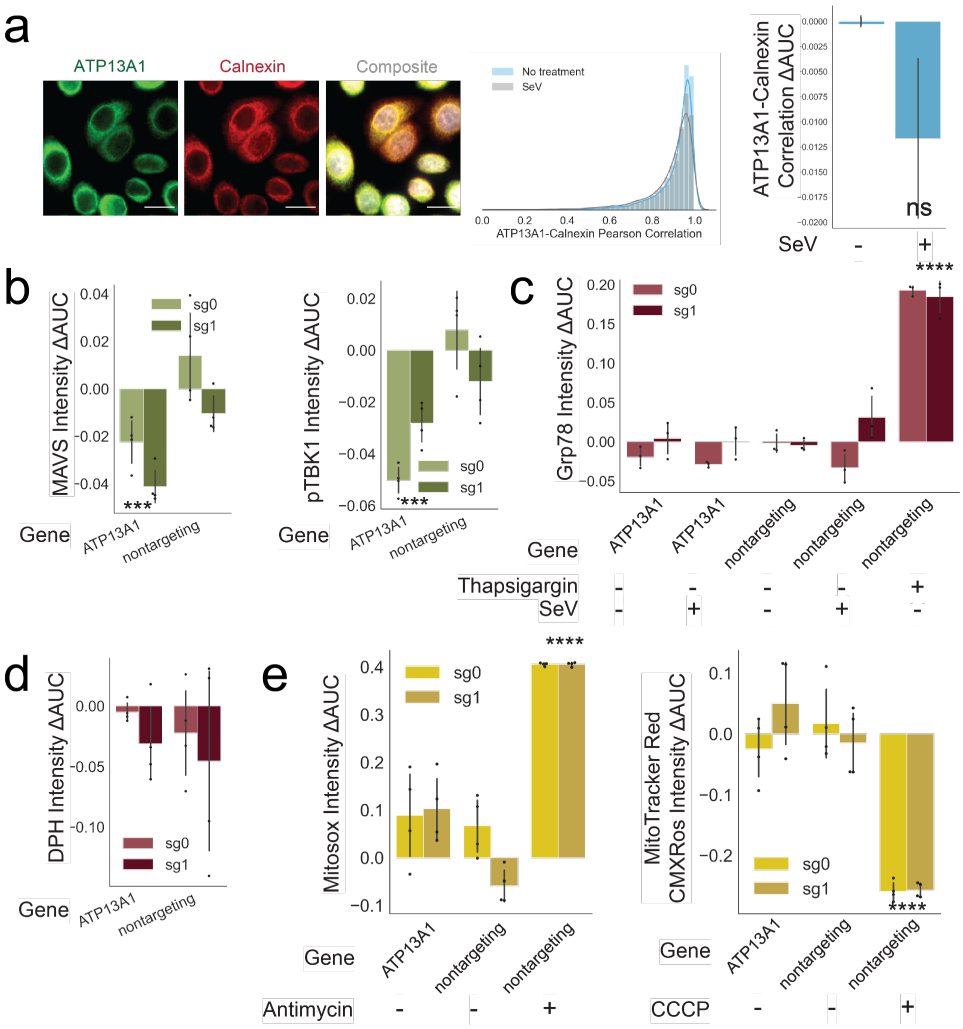

Supplementary Figure 5. (A) An ATP13A1 overexpression vector in HeLa cells is localized to the ER, as evidenced by colocalization with calnexin and localization is not significantly different in the presence of Sendai virus infection (normalized to median of no-infection condition). Two-sided p-values for a-e were calculated by computing the delta AUC for the feature of interest between cells in each well and non-targeting control cells (minimum n = 3,000); delta AUCs for all wells containing cells with an sgRNA of interest were then compared to non-targeting delta AUCs using a t test, p values were combined using Fisher's method and corrected using the Benjamini-Hochberg procedure. (B) MAVS and pTBK1 are decreased in HeLa cells in the presence of an ATP13A1 knockout during Sendai virus infection (C) Grp78 intensity is not increased in ATP13A1 knockout cells relative to non-targeting control cells in the presence or absence of Sendai virus treatment. 1 μM thapsigargin treatment for 24 hours was used as a positive control (D) Lipid droplet content, measured by 2 μM DPH staining, is not significantly different in ATP13A1 knockout cells relative to non-targeting control cells. (E). Mitochondrial ROS (Mitosox) and membrane potential (MitoTracker Red CMXRos) are not significantly altered in ATP13A1 cells relative to non-targeting control cells. 120 μM antimycin A and 200 μM CCCP treatments for 1 hour served as positive controls.

References

1. J. M. Dempster et al., Extracting Biological Insights from the Project Achilles Genome-Scale CRISPR Screens in Cancer Cell Lines. *bioRxiv* (2019).
2. R. M. Meyers *et al.*, Computational correction of copy-number effect improves specificity of CRISPR-Cas9 essentiality screens in cancer cells. *Nat. Genet.* **49**, 1779–1784 (2017).